Title
n + p ELASTIC SCATTERING DATA BETWEEN l820 AND 2090 MeV c.m. ENERGY

Authors
Kalmus, G.E.
Michael, W.
Birge, R.W.
et al.

Publication Date
1970-07-01

Submitted to Physical Review

UCRL-19775
Preprint

c. 2

π^+p ELASTIC SCATTERING DATA BETWEEN 1820 AND 2090 MeV c.m. ENERGY

G. E. Kalmus, W. Michael, and R. W. Birge

S. Y. Fung and A. Kernan

July 1970

AEC Contract No. W-7405-eng-48

LAWRENCE RADIATION LABORATORY
UNIVERSITY of CALIFORNIA BERKELEY

UCRL-19775

π^+p ELASTIC SCATTERING DATA BETWEEN 1820 AND 2090 MeV c.m. ENERGY*

G. E. Kalmus, W. Michael, and R. W. Birge

Lawrence Radiation Laboratory
University of California
Berkeley, California 94720

and

S. Y. Fung and A. Kernan

University of California
Riverside, California 92502

July 1970

ABSTRACT

Total and differential elastic cross-section data are presented at eight incident π^+ momenta: 1.28, 1.34, 1.40, 1.43, 1.55, 1.68, 1.77, and 1.84 GeV/c. These data were obtained from a hydrogen bubble chamber exposure at the Bevatron, and contain more than 65 000 events. This represents more than one and one-half times the world's data hitherto available in this energy region.

I. INTRODUCTION

We present total and differential cross sections for π^+p elastic scattering at eight incident π^+ momenta: 1.28, 1.34, 1.40, 1.43, 1.55, 1.68, 1.77, and 1.84 GeV/c. These data, by-products of an extensive investigation of inelastic π^+p scattering, represent more than 1.5 times the world's differential cross-section data, up to now, in this energy region.[1] They result from the measurement of about 230 000 "two-prong" interactions in the Lawrence Radiation Laboratory 72-inch and 25-inch bubble chambers. The range in the cosine of the production angle covered by the data is $-1.0 < \cos\theta^* < 0.98$ at the six higher momenta and $-1.0 < \cos\theta^* < 0.96$ at the two lower momenta, where θ^* is the angle in the c.m. system between the pion in the final state and the beam direction.

II. EXPERIMENTAL PROCEDURE

A. Beam

The π^+ beam used for the three momenta in the 72-inch chamber (1.34, 1.43, and 1.68 GeV/c) had a single stage of separation with two vertical slits, the second being used to clean up the beam close to the bubble chamber. The momentum bite of the beam was < ± 1%. The proton contamination of beam was negligible, and the μ^+ contamination was estimated to be 5 ± 3%. The beam used for the five momenta in the 25-inch chamber was the K67 beam, which had two stages of separation. The momentum bite was < ± 1%, the proton contamination was negligible, and the μ^+ contamination was estimated to be 3 ± 2%.

B. Scanning and Measuring

The film was scanned for two-pronged events and roads were made for the Lawrence Radiation Laboratory Flying-Spot Digitizer (FSD) in a single pass. Approximately 10% of the film was rescanned to obtain an overall scanning efficiency. Events with a short proton (< 2 cm projected length in space) were measured by using the "crutch point" mode. In this, the scanner digitizes, on the roadmaker, the end of the proton track as well as the vertex point in each view. These points are transferred directly into the geometry program where a vector in space is reconstructed by using these points. The magnitude and direction of this vector (and their errors) are used in the fitting program. For proton track lengths of > 1.5 cm projected (≈ 1 mm on film) it has been shown that the FSD has a constant (and high) efficiency. At five of the eight momenta all events that failed to get through the geometry program (FOG) were remeasured. These remeasurements were used to determine whether these events were biased. It was found that these events were consistent in angular distribution with those that went through on the first pass. However, both passes showed a small but measurable (with high statistics) bias against low-momentum backward pions which were also close in azimuth to the plane containing the optical axis and the beam direction. (This is further discussed in Section IIIB.) The measuring efficiency (defined as the number of events that pass geometry) divided by the number of events that had roads made was between 85 and 90% for each pass except for a small number of rolls in which, because of bad film (edge marks missing or light tracks), it was lower than this. The three momenta that were not remeasured were, in fact, on the high side of this range. The fact that the remeasurements are essentially unbiased is not surprising when the usual reasons for failure are examined. These are predominantly overlapping beam tracks, confused origins, and tracks going outside their roads--the last of which is usually due to badly measured fiducials (on the roadmaker).

In addition to the main scanning and measuring of the data, a subset of data was handled somewhat differently in order to obtain the total elastic cross section. This is described in Section IIIB.

Table I gives some of the parameters of the exposure.

III. DATA

A. Geometry and Kinematics

All events measured were processed through the FOG-CLOUDY system of programs for reconstruction and kinematic fitting. The resulting kinematics together with the ionization information obtained from the FSD was then input into FAIR, where the assignment of a particular reaction (π^+p, $\pi^+p\pi^0$, $\pi^+p\eta^0$, $\pi^+\pi^+n$) was made on the basis of both the kinematic χ^2 and an ionization χ^2. It was found that events that were kinematically ambiguous between a 4-c elastic hypothesis and any of the 1-c hypotheses were, in fact, always elastic scattering. This left only the small number of events that were ambiguous between $\pi^+p \rightarrow \pi^+p$ and $\pi^+p \rightarrow p\pi^+$, i.e., for which a good fit was obtained when either track was assumed to be a pion (and the other a proton). These events which occur when the lab momenta (and, therefore, the lab angles) of the two outgoing tracks are the same were resolved by means of the ionization measurements. It should be noted that although these events populate a single region in angular distribution, it is the same for either mass hypothesis, and so even if the wrong hypothesis is used no distortion of the angular distribution results.

B. Weighting of Events

Two biases are known to be present in the data.

1. In events with a small momentum transfer to the proton, the recoil proton is often so small as to be undetectable. Below about P_p = 100 MeV/c (3 mm in space) the scanning efficiency is very small. Between 100 MeV/c and about 250 MeV/c (7 cm in space) the scanning efficiency was found to depend on the azimuthal angle of the proton. This effect is illustrated clearly in fig. 1. This shows a scatter plot of cos θ^* versus ϕ, the azimuth of the proton around the beam direction. The zero in ϕ is defined as being in the plane containing the beam direction and the optic axis of the camera. Figure 1 shows this plot at one of our momenta (1.43 GeV/c) and for $0.9 < \cos\theta^* < 1.0$. The depletion of events around $\phi = 0$, π, and 2π is clearly seen, as is the fact that as cos θ^* decreases (and P_p increases) so the bias decreases. Since the cos θ^* distribution clearly should not depend on ϕ, we have used only part of the ϕ range (for $0.9 < \cos\theta^* < 1.0$). To determine how much of the ϕ range to use, projections of the kind shown in figs. 2a through 2d were used. These histograms show the projections of the plot in fig. 1 onto the ϕ axis for the regions of cos θ^* 0.98 to 0.96, 0.96 to 0.94, 0.94 to 0.92, and 0.92 to 0.90. An unbiased ϕ plot should be flat; this is a necessary but not sufficient condition. It is also necessary to establish that no events are missed uniformly in the flat region of histograms. This was checked by the rescan, where no bias towards protons of projected length > 7 mm in space (6 mm on scan table) was found. The maximum convenient values of cos θ^* which gave at least half the ϕ range (90 ± 45 deg and 270 ± 45 deg) with the above conditions were $\cos\theta^* = 0.96$ for our two lower momenta (1.28 and 1.34 GeV/c) and $\cos\theta^* = 0.98$ for the higher momenta. Clearly, as the beam momentum increases and cos θ^* decreases (and proton momentum increases) so the usable portion of ϕ increases.

2. A small bias in the data also exists in the backward direction, i.e., for $-1.0 < \cos\theta^*$ < -0.95. This can be seen in fig. 3, which is a histogram of ϕ for the region $-1.0 < \cos\theta^*$ < -0.95 at 1.55 GeV/c. The events missing have backward pions (in both c.m. and lab) which, when combined with a ϕ of close to 0 or π, lie right on top of the beam track near the vertex and therefore have a slightly higher-than-normal failure rate.

The bins that are weighted for the ϕ bias are shown in Tables IIa-h. The fraction of the ϕ range used in each bin can be obtained by dividing the unweighted number by the weighted number.

IV. RESULTS

A. Total Elastic Cross Sections

The total elastic cross sections were obtained in the following way:

1. A sample of film at each momentum containing between 400 and 800 accepted elastic events was carefully rescanned.

2. Beam tracks were counted every 20 frames on the 25-inch chamber film (every 10 frames on 72-inch film) for these rolls. From this total we calculated the π^+ path length (L) in these rolls, taking into account the loss of beam due to interactions (based on the known π^+ total cross section) and the μ^+ contamination.

3. All two-prongs found in the first scan were traced through the FSD (HAZE), geometry (FOG), kinematics (CLOUDY), and library (FAIR) programs in order to determine the throughput efficiency of the system.

4. About 150 events at each momentum from the above sample of film that were within the fiducial volume but failed to fit any of the hypotheses π^+p, $p\pi^+$, $\pi^+p\pi^0$, $p\pi^+\pi^0$, $\pi^+\pi^+n$,

$\pi^+ p\eta$, or $p\pi^+\eta$ with a satisfactory χ^2 were remeasured in order to determine the measuring efficiency for events that go through geometry.

We now define the following quantities for the sample of film at each momentum:

N_f, the number of accepted elastic events in the sample of film;

L, the total π^+ path length taking into account the μ^+ contamination and beam loss due to interactions (based on the known total cross sections);

ϵ_1, the scanning efficiency of the first scan;

ϵ_2, the throughput efficiency of the system;

ϵ_3, the measuring efficiency for elastic events.

(It should be noted that the way in which ϵ_3 was measured ensured that ϵ_3 included both the effect of bad first measures and the effect of the tail of the first-measure χ^2 distribution.)

The total number of elastic scattering (N_T) in the sample of film at each momentum is given by

$$N_T = N_f \left(\frac{1}{\epsilon_1} \times \frac{1}{\epsilon_2} \times \frac{1}{\epsilon_3}\right) \times c,$$

where c is the ratio of the total number (N_t) of elastic events accepted in the <u>entire</u> film (at one momentum) to the area (N) under the fitted Legendre polynomial (see Section B).

The total elastic cross section is given by

$$\sigma_{el} = \frac{27\,800}{L} \times N_T \text{ mb, where L is in cm}$$

(at the operating conditions of the chamber 1 mb is equivalent to 27 800 cm of path length).

The error in σ_{el} has been calculated by combining the following effects:

(a)	Statistical error on N_f	≈5%
(b)	Statistical error on number of beam track counted	≈2.5%
(c)	Error on μ contamination	≈2%
(d)	Error on ϵ_1	≈2%
(e)	Error on ϵ_2	≈1%
(f)	Error on ϵ_3	≈2%
(g)	Error on N_t	≈1%
(h)	Error on N	≈1%

The last of these was estimated by increasing the order of fit by one and seeing how much the area under the curve changed as well as by the usual propagation of errors.

Thus it can be seen that the statistical error on N_f, and the other errors combined, contribute equally to the final error of ≈7%.

Table III and fig. 4 show the elastic cross sections obtained.

B. <u>Angular Distributions</u>

Table II a-h and figs. 5 a-h show the angular distributions at the various momenta. In figs. 5a-h the histograms of weighted events have been plotted in such a way that equal areas correspond to equal number of events, since the bin size above $\cos\theta^* = 0.90$ has been decreased. These data, in the bins shown, were then fitted with a Legendre series, using a least-squares method, in the range $-1.0 < \cos\theta^* < 0.98$ for the six higher momenta and $-1.0 < \cos\theta^* < 0.96$ for the two lower momenta. The expansion used was

$$\frac{dN}{d(\cos\theta^*)} = 1/2 \sum_{n=0}^{8} A_n P_n (\cos\theta^*),$$

Table IV and fig. 6 give the values of coefficients of the Legendre series normalized to the zeroth order, A_n/A_0 up to A_8/A_0. At no momenta was a higher order needed to fit the data. A typical curve of χ^2 divided by degrees of freedom is shown in fig. 7. The area under the fitted curve is proportional to the total number N ($=A_0$) of elastic events (at all angles).

The differential cross sections in mb/sr given in Table II are directly proportional to the number of events per unit interval in $\cos\theta^*$. Strictly speaking, they should be interpreted as a mean for each bin, although clearly, since the forward bins have been split into fine intervals, a very good approximation is to use the midpoint of each bin.

The constant of proportionality is given by

$$\left.\frac{d\sigma}{d\Omega}\right|_{\substack{\text{averaged}\\ \text{over bin i}}} = \frac{N_i}{N} \times \sigma_{el} \times \frac{1}{\Delta \cos \theta^*_i} \frac{1}{2\pi},$$

where N_i is the number of events in bin i (or weighted number), and $\Delta \cos \theta^*_i$ is the bin width. The error in σ_{el} has not been progated into $d\sigma/d\Omega$, since it affects only the overall normalization and not the relative error between bins.

V. DISCUSSION

The purpose of this paper is to present our data in such a form that they may readily be used in phase-shift analyses. The differential cross sections are of accuracy comparable to or greater than any in the literature in this energy region, and have greater range (in cos θ^*); we hope they will be particularly useful. Qualitatively, they appear to agree with available published data. The total elastic cross sections presented are also in good agreement with those in the literature, (see fig. 4) with the possible exception of our point at 1.55 GeV/c. The general method used to determine the total elastic cross section was also the one used to determine the various inelastic-channel cross sections, for which it is more appropriate. In this method it is very difficult to determine systematic effects to within less than 4 or 5%, and therefore we decided to match our statistical error to this.

VI. ACKNOWLEDGMENTS

We thank Howard White, Dennis Hall, and Loren Shaltz of the Data Handling Group for their efforts in processing the data, and are grateful to the scanners and measurers of the Powell-Birge group, particularly, Toni Woodford, who did much of the work necessary in determining the total elastic cross sections. Finally, we acknowledge the efforts of Bert Albrecht, John Visser, Charlotte Scales, and Maggie Morley, who were involved in the all-important bookkeeping aspects of this experiment.

FOOTNOTE AND REFERENCE

*Work done under auspices of the U. S. Atomic Energy Commission.

1. G. Giacomelli, P. Pini, and S. Stagni, A Compilation of Pion-Nucleon Scattering Data, CERN Preprint CERN/HERA 69-1 (unpublished).

Table I. Parameters of this exposure.

Beam momentum (GeV/c)	Total energy in c.m. (GeV)	Number of pictures measured	Number of 2-prongs measured
1.28	1.821	35 000	13 000
1.34	1.850	28 000[a]	39 000
1.40	1.881	50 000	21 000
1.43	1.896	22 000[a]	31 000
1.55	1.955	121 000	40 000
1.68	2.016	30 000[a]	37 000
1.77	2.057	122 000	24 000
1.84	2.089	119 000	25 000

a. 72-Inch chamber pictures; others are 25-inch chamber pictures.

Table II. Numbers of events in the angular distributions and differential cross sections, and errors (Part a). 1.28 (GeV/c)

Cos θ* Interval	Number of Weighted Events	Number of Unweighted Events	Error in Number of Weighted Events	Cross Section mb/sr	Error in Cross Section mb/sr
-1.00 -.95	136.0	136.0	11.662	1.515	.130
-.95 -.90	113.0	113.0	10.630	1.259	.118
-.90 -.85	76.0	76.0	8.718	.847	.097
-.85 -.80	73.0	73.0	8.544	.813	.095
-.80 -.75	58.0	58.0	7.616	.646	.085
-.75 -.70	48.0	48.0	6.928	.535	.077
-.70 -.65	53.0	53.0	7.280	.591	.081
-.65 -.60	57.0	57.0	7.550	.635	.084
-.60 -.55	83.0	83.0	9.110	.925	.102
-.55 -.50	67.0	67.0	8.185	.747	.091
-.50 -.45	70.0	70.0	8.367	.780	.093
-.45 -.40	72.0	72.0	8.485	.802	.095
-.40 -.35	70.0	70.0	8.367	.780	.093
-.35 -.30	72.0	72.0	8.485	.802	.095
-.30 -.25	55.0	55.0	7.416	.613	.083
-.25 -.20	40.0	40.0	6.325	.446	.070
-.20 -.15	35.0	35.0	5.916	.390	.066
-.15 -.10	39.0	39.0	6.245	.435	.070
-.10 -.05	27.0	27.0	5.196	.301	.058
-.05 0.00	23.0	23.0	4.796	.256	.053
0.00 .05	25.0	25.0	5.000	.279	.056
.05 .10	24.0	24.0	4.899	.267	.055
.10 .15	20.0	20.0	4.472	.223	.050
.15 .20	15.0	15.0	3.873	.167	.043
.20 .25	30.0	30.0	5.477	.334	.061
.25 .30	37.0	37.0	6.083	.412	.068
.30 .35	34.0	34.0	5.831	.379	.065
.35 .40	43.0	43.0	6.557	.479	.073
.40 .45	62.0	62.0	7.874	.691	.088
.45 .50	70.0	70.0	8.367	.780	.093
.50 .55	84.0	84.0	9.165	.936	.102
.55 .60	99.0	99.0	9.950	1.103	.111
.60 .65	125.0	125.0	11.180	1.393	.125
.65 .70	158.0	158.0	12.570	1.760	.140
.70 .75	191.0	191.0	13.820	2.128	.154
.75 .80	253.0	253.0	15.906	2.819	.177
.80 .85	288.0	288.0	16.971	3.209	.189
.85 .90	379.0	379.0	19.468	4.223	.217
.90 .92	193.0	161.0	15.211	5.376	.424
.92 .94	209.0	170.0	16.030	5.822	.447
.94 .96	290.0	193.0	20.875	8.078	.581

Table II, Part b 1.34 (GeV/c)

Cos θ* Interval		Number of Weighted Events (Ni)	Number of Unweighted Events	Error in Number of Weighted Events	Cross Section mb/sr	Error in Cross Section mb/sr
-1.00	-.95	476.0	445.0	22.565	2.213	.105
-.95	-.90	302.0	302.0	17.378	1.404	.081
-.90	-.85	222.0	222.0	14.900	1.032	.069
-.85	-.80	144.0	144.0	12.000	.670	.056
-.80	-.75	157.0	157.0	12.530	.730	.058
-.75	-.70	125.0	125.0	11.180	.581	.052
-.70	-.65	163.0	163.0	12.767	.758	.059
-.65	-.60	169.0	169.0	13.000	.786	.060
-.60	-.55	196.0	196.0	14.000	.911	.065
-.55	-.50	211.0	211.0	14.526	.981	.068
-.50	-.45	198.0	198.0	14.071	.921	.065
-.45	-.40	214.0	214.0	14.629	.995	.068
-.40	-.35	222.0	222.0	14.900	1.032	.069
-.35	-.30	208.0	208.0	14.422	.967	.067
-.30	-.25	195.0	195.0	13.964	.907	.065
-.25	-.20	165.0	165.0	12.845	.767	.060
-.20	-.15	152.0	152.0	12.329	.707	.057
-.15	-.10	137.0	137.0	11.705	.637	.054
-.10	-.05	114.0	114.0	10.677	.530	.050
-.05	0.00	96.0	96.0	9.798	.446	.046
0.00	.05	56.0	56.0	7.483	.260	.035
.05	.10	52.0	52.0	7.211	.242	.034
.10	.15	61.0	61.0	7.810	.284	.036
.15	.20	54.0	54.0	7.348	.251	.034
.20	.25	29.0	29.0	5.385	.135	.025
.25	.30	72.0	72.0	8.485	.335	.039
.30	.35	74.0	74.0	8.602	.344	.040
.35	.40	95.0	95.0	9.747	.442	.045
.40	.45	119.0	119.0	10.909	.553	.051
.45	.50	137.0	137.0	11.705	.637	.054
.50	.55	180.0	180.0	13.416	.837	.062
.55	.60	217.0	217.0	14.731	1.009	.068
.60	.65	254.0	254.0	15.937	1.181	.074
.65	.70	322.0	322.0	17.944	1.497	.083
.70	.75	450.0	450.0	21.213	2.092	.099
.75	.80	553.0	553.0	23.516	2.571	.109
.80	.85	770.0	770.0	27.749	3.580	.129
.85	.90	1083.0	1083.0	32.909	5.035	.153
.90	.92	501.0	334.0	27.414	5.823	.319
.92	.94	573.0	382.0	29.317	6.660	.341
.94	.96	747.0	498.0	33.474	8.683	.389

Table II, Part c 1.40(GeV/c)

Cos θ^* Interval	Number of Weighted Events	Number of Unweighted Events	Error in Number of Weighted Events	Cross Section mb/sr	Error in Cross Section mb/sr
-1.00 -.95	267.0	267.0	16.340	1.842	.113
-.95 -.90	181.0	181.0	13.454	1.249	.093
-.90 -.85	126.0	126.0	11.225	.869	.077
-.85 -.80	79.0	79.0	8.888	.545	.061
-.80 -.75	109.0	109.0	10.440	.752	.072
-.75 -.70	94.0	94.0	9.695	.648	.067
-.70 -.65	115.0	115.0	10.724	.793	.074
-.65 -.60	114.0	114.0	10.677	.786	.074
-.60 -.55	119.0	119.0	10.909	.821	.075
-.55 -.50	155.0	155.0	12.450	1.069	.086
-.50 -.45	141.0	141.0	11.874	.973	.082
-.45 -.40	183.0	183.0	13.528	1.262	.093
-.40 -.35	175.0	175.0	13.229	1.207	.091
-.35 -.30	158.0	158.0	12.570	1.090	.087
-.30 -.25	167.0	167.0	12.923	1.152	.089
-.25 -.20	126.0	126.0	11.225	.869	.077
-.20 -.15	106.0	106.0	10.296	.731	.071
-.15 -.10	83.0	83.0	9.110	.573	.063
-.10 -.05	84.0	84.0	9.165	.579	.063
-.05 0.00	67.0	67.0	8.185	.462	.056
0.00 .05	70.0	70.0	8.367	.483	.058
.05 .10	50.0	50.0	7.071	.345	.049
.10 .15	48.0	48.0	6.928	.331	.048
.15 .20	39.0	39.0	6.245	.269	.043
.20 .25	43.0	43.0	6.557	.297	.045
.25 .30	36.0	36.0	6.000	.248	.041
.30 .35	31.0	31.0	5.568	.214	.038
.35 .40	37.0	37.0	6.083	.255	.042
.40 .45	41.0	41.0	6.403	.283	.044
.45 .50	40.0	40.0	6.325	.276	.044
.50 .55	44.0	44.0	6.633	.304	.046
.55 .60	69.0	69.0	8.307	.476	.057
.60 .65	90.0	90.0	9.487	.621	.065
.65 .70	119.0	119.0	10.909	.821	.075
.70 .75	210.0	210.0	14.491	1.449	.100
.75 .80	323.0	323.0	17.972	2.228	.124
.80 .85	515.0	515.0	22.694	3.552	.157
.85 .90	789.0	789.0	28.089	5.442	.194
.90 .92	367.0	367.0	19.157	6.329	.330
.92 .94	444.0	369.0	23.114	7.657	.399
.94 .96	553.0	461.0	25.756	9.536	.444
.96 .98	615.0	409.0	30.410	10.605	.524

Table II, Part d 1.43(GeV/c)

Cos θ^* Interval	Number of Weighted Events	Number of Unweighted Events	Error in Number of Weighted Events	Cross Section mb/sr	Error in Cross Section mb/sr
-1.00 -.95	346.0	303.0	19.877	2.208	.127
-.95 -.90	242.0	242.0	15.556	1.544	.099
-.90 -.85	137.0	137.0	11.705	.874	.075
-.85 -.80	99.0	99.0	9.950	.632	.063
-.80 -.75	106.0	106.0	10.296	.676	.066
-.75 -.70	113.0	113.0	10.630	.721	.068
-.70 -.65	148.0	148.0	12.166	.944	.078
-.65 -.60	175.0	175.0	13.229	1.117	.084
-.60 -.55	177.0	177.0	13.304	1.129	.085
-.55 -.50	196.0	196.0	14.000	1.251	.089
-.50 -.45	212.0	212.0	14.560	1.353	.093
-.45 -.40	214.0	214.0	14.629	1.365	.093
-.40 -.35	219.0	219.0	14.799	1.397	.094
-.35 -.30	195.0	195.0	13.964	1.244	.089
-.30 -.25	179.0	179.0	13.379	1.142	.085
-.25 -.20	186.0	186.0	13.638	1.187	.087
-.20 -.15	138.0	138.0	11.747	.880	.075
-.15 -.10	126.0	126.0	11.225	.804	.072
-.10 -.05	113.0	113.0	10.630	.721	.068
-.05 0.00	87.0	87.0	9.327	.555	.060
0.00 .05	82.0	82.0	9.055	.523	.058
.05 .10	62.0	62.0	7.874	.396	.050
.10 .15	56.0	56.0	7.483	.357	.048
.15 .20	45.0	45.0	6.708	.287	.043
.20 .25	45.0	45.0	6.708	.287	.043
.25 .30	43.0	43.0	6.557	.274	.042
.30 .35	36.0	36.0	6.000	.230	.038
.35 .40	52.0	52.0	7.211	.332	.046
.40 .45	49.0	49.0	7.000	.313	.045
.45 .50	50.0	50.0	7.071	.319	.045
.50 .55	56.0	56.0	7.483	.357	.048
.55 .60	86.0	86.0	9.274	.549	.059
.60 .65	147.0	147.0	12.124	.938	.077
.65 .70	193.0	193.0	13.892	1.231	.089
.70 .75	281.0	281.0	16.763	1.793	.107
.75 .80	430.0	430.0	20.736	2.744	.132
.80 .85	673.0	673.0	25.942	4.294	.166
.85 .90	930.0	930.0	30.496	5.934	.195
.90 .92	541.0	361.0	28.474	8.629	.454
.92 .94	671.0	447.0	31.737	10.703	.506
.94 .96	704.0	469.0	32.508	11.229	.519
.96 .98	798.0	399.0	39.950	12.729	.637

Table II, Part e 1.55 (GeV/c)

Cos θ^* Interval		Number of Weighted Events	Number of Unweighted Events	Error in Number of Weighted Events	Cross Section mb/sr	Error in Cross Section mb/sr
-1.00	-.95	339.0	285.0	20.081	.978	.058
-.95	-.90	196.0	178.0	14.691	.565	.042
-.90	-.85	141.0	141.0	11.874	.407	.034
-.85	-.80	123.0	123.0	11.091	.355	.032
-.80	-.75	126.0	126.0	11.225	.363	.032
-.75	-.70	175.0	175.0	13.229	.505	.038
-.70	-.65	168.0	168.0	12.961	.485	.037
-.65	-.60	209.0	209.0	14.457	.603	.042
-.60	-.55	269.0	269.0	16.401	.776	.047
-.55	-.50	298.0	298.0	17.263	.860	.050
-.50	-.45	275.0	275.0	16.583	.793	.048
-.45	-.40	338.0	338.0	18.385	.975	.053
-.40	-.35	321.0	321.0	17.916	.926	.052
-.35	-.30	274.0	274.0	16.553	.790	.048
-.30	-.25	259.0	259.0	16.093	.747	.046
-.25	-.20	269.0	269.0	16.401	.776	.047
-.20	-.15	245.0	245.0	15.652	.707	.045
-.15	-.10	198.0	198.0	14.071	.571	.041
-.10	-.05	175.0	175.0	13.229	.505	.038
-.05	0.00	146.0	146.0	12.083	.421	.035
0.00	.05	141.0	141.0	11.874	.407	.034
.05	.10	138.0	138.0	11.747	.398	.034
.10	.15	128.0	128.0	11.314	.369	.033
.15	.20	112.0	112.0	10.583	.323	.031
.20	.25	87.0	87.0	9.327	.251	.027
.25	.30	80.0	80.0	8.944	.231	.026
.30	.35	53.0	53.0	7.280	.153	.021
.35	.40	49.0	49.0	7.000	.141	.020
.40	.45	36.0	36.0	6.000	.104	.017
.45	.50	34.0	34.0	5.831	.098	.017
.50	.55	35.0	35.0	5.916	.101	.017
.55	.60	57.0	57.0	7.550	.164	.022
.60	.65	103.0	103.0	10.149	.297	.029
.65	.70	192.0	192.0	13.856	.554	.040
.70	.75	379.0	379.0	19.468	1.093	.056
.75	.80	677.0	677.0	26.019	1.953	.075
.80	.85	1050.0	1050.0	32.404	3.029	.093
.85	.90	1846.0	1846.0	42.965	5.325	.124
.90	.92	929.0	774.0	33.392	6.699	.241
.92	.94	1033.0	861.0	35.205	7.449	.254
.94	.96	1250.0	1042.0	38.724	9.014	.279
.96	.98	1392.0	928.0	45.695	10.038	.330

Table II, Part f 1.68(GeV/c)

Cos θ* Interval	Number of Weighted Events	Number of Unweighted Events	Error in Number of Weighted Events	Cross Section mb/sr	Error in Cross Section mb/sr
-1.00 -.95	119.0	114.0	11.145	.489	.046
-.95 -.90	73.0	73.0	8.544	.300	.035
-.90 -.85	67.0	67.0	8.185	.275	.034
-.85 -.80	41.0	41.0	6.403	.168	.026
-.80 -.75	53.0	53.0	7.280	.218	.030
-.75 -.70	61.0	61.0	7.810	.250	.032
-.70 -.65	75.0	75.0	8.660	.308	.036
-.65 -.60	117.0	117.0	10.817	.480	.044
-.60 -.55	136.0	136.0	11.662	.558	.048
-.55 -.50	157.0	157.0	12.530	.645	.051
-.50 -.45	167.0	167.0	12.923	.686	.053
-.45 -.40	138.0	138.0	11.747	.567	.048
-.40 -.35	152.0	152.0	12.329	.624	.051
-.35 -.30	173.0	173.0	13.153	.710	.054
-.30 -.25	175.0	175.0	13.229	.719	.054
-.25 -.20	152.0	152.0	12.329	.624	.051
-.20 -.15	139.0	139.0	11.790	.571	.048
-.15 -.10	100.0	100.0	10.000	.411	.041
-.10 -.05	114.0	114.0	10.677	.468	.044
-.05 0.00	82.0	82.0	9.055	.337	.037
0.00 .05	105.0	105.0	10.247	.431	.042
.05 .10	69.0	69.0	8.307	.283	.034
.10 .15	79.0	79.0	8.888	.324	.036
.15 .20	73.0	73.0	8.544	.300	.035
.20 .25	77.0	77.0	8.775	.316	.036
.25 .30	81.0	81.0	9.000	.333	.037
.30 .35	59.0	59.0	7.681	.242	.032
.35 .40	59.0	59.0	7.681	.242	.032
.40 .45	39.0	39.0	6.245	.160	.026
.45 .50	48.0	48.0	6.928	.197	.028
.50 .55	34.0	34.0	5.831	.140	.024
.55 .60	42.0	42.0	6.481	.172	.027
.60 .65	73.0	73.0	8.544	.300	.035
.65 .70	150.0	150.0	12.247	.616	.050
.70 .75	282.0	282.0	16.793	1.158	.069
.75 .80	482.0	482.0	21.954	1.979	.090
.80 .85	754.0	754.0	27.459	3.096	.113
.85 .90	1206.0	1206.0	34.728	4.952	.143
.90 .92	624.0	520.0	27.364	6.405	.281
.92 .94	752.0	627.0	30.032	7.719	.308
.94 .96	974.0	649.0	38.233	9.998	.392
.96 .98	1050.0	525.0	45.826	10.778	.470

Table II, Part g 1.77(GeV/c)

Cos θ* Interval	Number of Weighted Events	Number of Unweighted Events	Error in Number of Weighted Events	Cross Section mb/sr	Error in Cross Section mb/sr
-1.00 -.95	72.0	68.0	8.731	.210	.026
-.95 -.90	51.0	51.0	7.141	.149	.021
-.90 -.85	24.0	24.0	4.899	.070	.014
-.85 -.80	37.0	37.0	6.083	.108	.018
-.80 -.75	38.0	38.0	6.164	.111	.018
-.75 -.70	65.0	65.0	8.062	.190	.024
-.70 -.65	74.0	74.0	8.602	.216	.025
-.65 -.60	85.0	85.0	9.220	.248	.027
-.60 -.55	109.0	109.0	10.440	.318	.030
-.55 -.50	134.0	134.0	11.576	.391	.034
-.50 -.45	127.0	127.0	11.269	.371	.033
-.45 -.40	129.0	129.0	11.358	.377	.033
-.40 -.35	167.0	167.0	12.923	.488	.038
-.35 -.30	127.0	127.0	11.269	.371	.033
-.30 -.25	142.0	142.0	11.916	.415	.035
-.25 -.20	120.0	120.0	10.954	.351	.032
-.20 -.15	106.0	106.0	10.296	.310	.030
-.15 -.10	87.0	87.0	9.327	.254	.027
-.10 -.05	120.0	120.0	10.954	.351	.032
-.05 0.00	106.0	106.0	10.296	.310	.030
0.00 .05	102.0	102.0	10.100	.298	.030
.05 .10	117.0	117.0	10.817	.342	.032
.10 .15	99.0	99.0	9.950	.289	.029
.15 .20	88.0	88.0	9.381	.257	.027
.20 .25	120.0	120.0	10.954	.351	.032
.25 .30	74.0	74.0	8.602	.216	.025
.30 .35	83.0	83.0	9.110	.242	.027
.35 .40	88.0	88.0	9.381	.257	.027
.40 .45	57.0	57.0	7.550	.166	.022
.45 .50	57.0	57.0	7.550	.166	.022
.50 .55	57.0	57.0	7.550	.166	.022
.55 .60	94.0	94.0	9.695	.275	.028
.60 .65	115.0	115.0	10.724	.336	.031
.65 .70	200.0	200.0	14.142	.584	.041
.70 .75	358.0	358.0	18.921	1.046	.055
.75 .80	566.0	566.0	23.791	1.653	.069
.80 .85	954.0	954.0	30.887	2.787	.090
.85 .90	1365.0	1365.0	36.946	3.987	.108
.90 .92	706.0	706.0	26.571	5.156	.194
.92 .94	876.0	730.0	32.422	6.397	.237
.94 .96	952.0	794.0	33.785	6.952	.247
.96 .98	1260.0	840.0	43.474	9.201	.317

Table II, Part h 1.84 (GeV/c)

Cos θ^* Interval	Number of Weighted Events	Number of Unweighted Events	Error in Number of Weighted Events	Cross Section mb/sr	Error in Cross Section mb/sr
-1.00 -.95	31.0	31.0	5.568	.115	.021
-.95 -.90	16.0	16.0	4.000	.060	.015
-.90 -.85	20.0	20.0	4.472	.075	.017
-.85 -.80	14.0	14.0	3.742	.052	.014
-.80 -.75	22.0	22.0	4.690	.082	.017
-.75 -.70	32.0	32.0	5.657	.119	.021
-.70 -.65	31.0	31.0	5.568	.115	.021
-.65 -.60	45.0	45.0	6.708	.168	.025
-.60 -.55	70.0	70.0	8.367	.261	.031
-.55 -.50	66.0	66.0	8.124	.246	.030
-.50 -.45	79.0	79.0	8.888	.294	.033
-.45 -.40	109.0	109.0	10.440	.406	.039
-.40 -.35	80.0	80.0	8.944	.298	.033
-.35 -.30	90.0	90.0	9.487	.335	.035
-.30 -.25	99.0	99.0	9.950	.369	.037
-.25 -.20	73.0	73.0	8.544	.272	.032
-.20 -.15	68.0	68.0	8.246	.253	.031
-.15 -.10	71.0	71.0	8.426	.264	.031
-.10 -.05	73.0	73.0	8.544	.272	.032
-.05 0.00	74.0	74.0	8.602	.276	.032
0.00 .05	72.0	72.0	8.485	.268	.032
.05 .10	73.0	73.0	8.544	.272	.032
.10 .15	67.0	67.0	8.185	.250	.030
.15 .20	74.0	74.0	8.602	.276	.032
.20 .25	65.0	65.0	8.062	.242	.030
.25 .30	98.0	98.0	9.899	.365	.037
.30 .35	61.0	61.0	7.810	.227	.029
.35 .40	66.0	66.0	8.124	.246	.030
.40 .45	51.0	51.0	7.141	.190	.027
.45 .50	52.0	52.0	7.211	.194	.027
.50 .55	46.0	46.0	6.782	.171	.025
.55 .60	67.0	67.0	8.185	.250	.030
.60 .65	106.0	106.0	10.296	.395	.038
.65 .70	155.0	155.0	12.450	.577	.046
.70 .75	250.0	250.0	15.811	.931	.059
.75 .80	393.0	393.0	19.824	1.464	.074
.80 .85	630.0	630.0	25.100	2.347	.094
.85 .90	992.0	992.0	31.496	3.695	.117
.90 .92	516.0	516.0	22.716	4.806	.212
.92 .94	587.0	489.0	26.545	5.467	.247
.94 .96	747.0	623.0	29.928	6.957	.279
.96 .98	803.0	535.0	34.717	7.478	.323

Table III. Numbers of events and cross sections at the various momenta.

Beam momentum (GeV/c)	N_f Number of good elastic events found within fiducial volume	Number of events within the accepted range in cos θ^* and ϕ	Number of weighted events within the accepted range of cos θ^*	N_t Number of events under the fitted curve $-1<\cos\theta^*<1$	Cross-section (mb)
1.28	4 031	3 730	3 832	4 428	15.5 ± 1.1
1.34	10 871	9 627	10 265	11 981	17.5 ± 1.2
1.40	7 333	6 849	7 096	7 891	17.1 ± 1.2
1.43	9 239	8 357	9 438	10 327	20.7 ± 1.5
1.55	14 205	13 274	14 345	16 001	15.2 ± 1.0
1.68	9 451	8 319	9 403	10 543	13.6 ± 1.0
1.77	10 794	9 580	10 308	11 550	11.6 ± 0.8
1.84	7 246	6 644	7 134	8 031	9.9 ± 0.7

Table IV. Legendre A coefficients.

	$P\pi^+$ (GeV/c)							
	1.28	1.34	1.40	1.43	1.55	1.68	1.77	1.84
$A1/_{Ao}$	1.185 (±0.050)	1.099 (±0.031)	1.127 (±0.032)	1.153 (±0.030)	1.406 (±0.023)	1.695 (±0.031)	1.878 (±0.028)	1.961 (±0.033)
$A2/_{Ao}$	1.961 (±0.072)	2.019 (±0.045)	2.112 (±0.046)	2.124 (±0.044)	2.245 (±0.034)	2.375 (±0.045)	2.425 (±0.041)	2.428 (±0.049)
$A3/_{Ao}$	1.367 (±0.088)	1.613 (±0.055)	2.124 (±0.055)	2.146 (±0.053)	2.615 (±0.040)	2.787 (±0.054)	2.741 (±0.048)	2.729 (±0.058)
$A4/_{Ao}$	0.926 (±0.102)	1.298 (±0.063)	1.733 (±0.061)	1.728 (±0.059)	2.062 (±0.044)	2.212 (±0.059)	2.161 (±0.053)	2.178 (±0.063)
$A5/_{Ao}$	0.234 (±0.105)	0.293 (±0.063)	0.616 (±0.062)	0.584 (±0.059)	0.974 (±0.043)	1.215 (±0.057)	1.257 (±0.052)	1.301 (±0.063)
$A6/_{Ao}$	0.533 (±0.101)	0.768 (±0.061)	0.816 (±0.059)	0.877 (±0.055)	0.855 (±0.039)	0.895 (±0.052)	0.766 (±0.048	0.762 (±0.058)
$A7/_{Ao}$	0.104 (±0.081)	0.201 (±0.048)	0.105 (±0.050)	0.096 (±0.045)	0.108 (±0.033)	0.170 (±0.044)	0.111 (±0.042)	0.157 (±0.051)
$A8/_{Ao}$	-0.013 (±0.073)	0.074 (±0.044)	-0.049 (±0.049)	0.045 (±0.044)	-0.013 (±0.032)	-0.085 (±0.038)	-0.025 (±0.033)	-0.060 (±0.038)
$\chi^2/_{D.F.}$	$^{31}/_{33}$	$^{43}/_{33}$	$^{37}/_{34}$	$^{28}/_{34}$	$^{45}/_{34}$	$^{44}/_{34}$	$^{56}/_{34}$	$^{35}/_{34}$

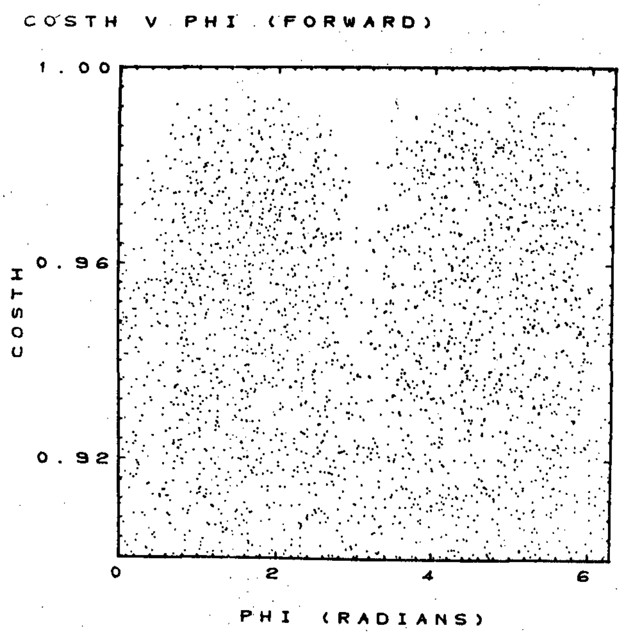

Fig. 1. Scatter plot of ϕ versus $\cos\theta^*$ at 1.43 GeV/c for forward scattering angles ($0.9 < \cos\theta^* < 1.0$).

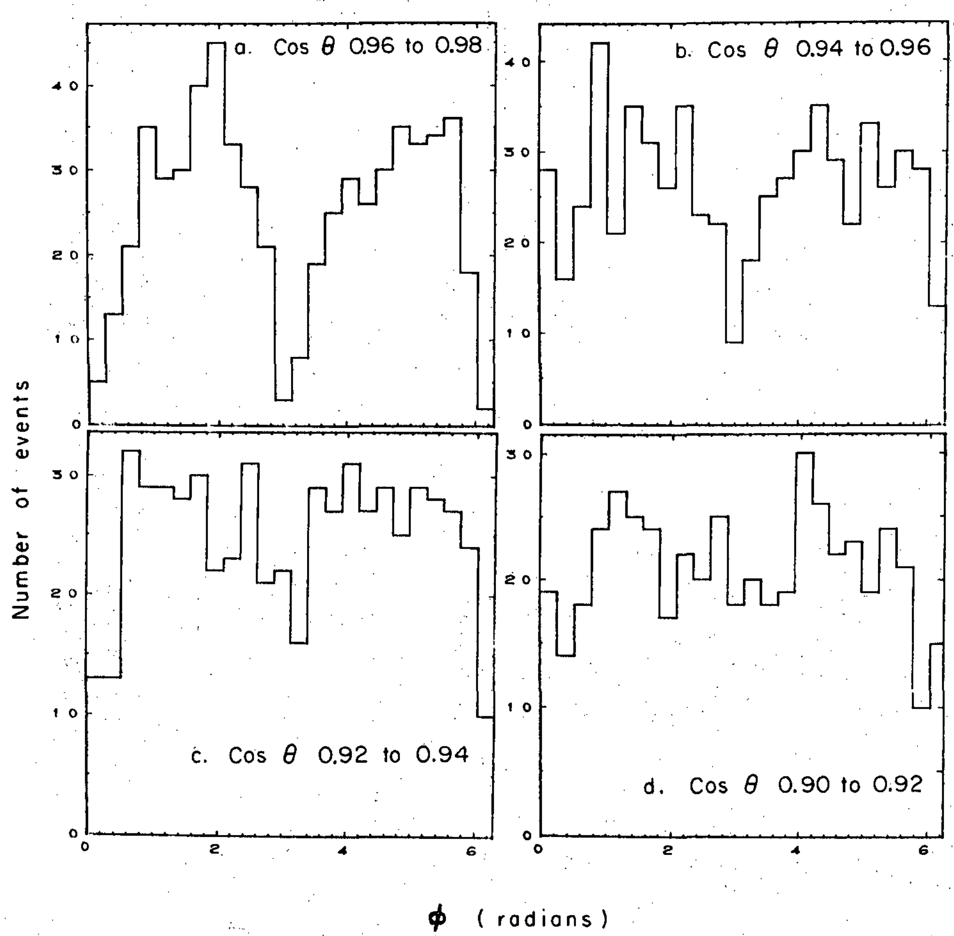

Fig. 2. Histograms of ϕ for various regions of of $\cos\theta^*$ at 1.43 GeV/c.

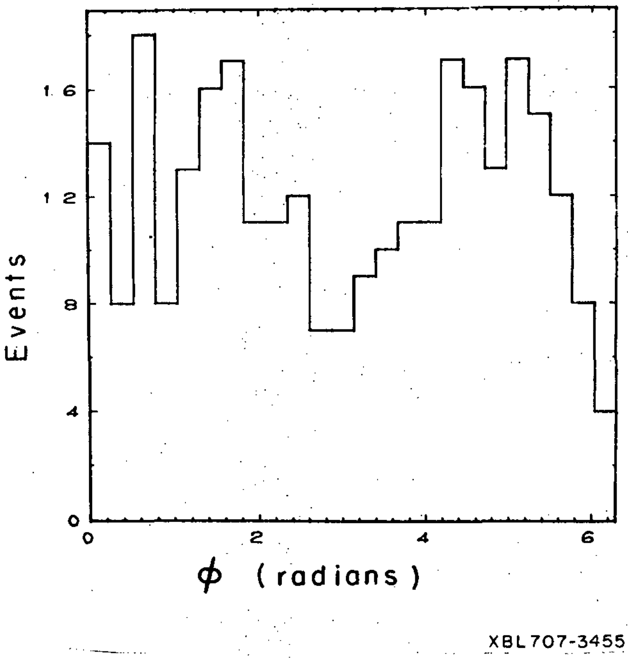

Fig. 3. Histogram of ϕ for $-1.0 < \cos\theta^* < -0.9$, i.e., the backward direction, at 1.55 GeV/c.

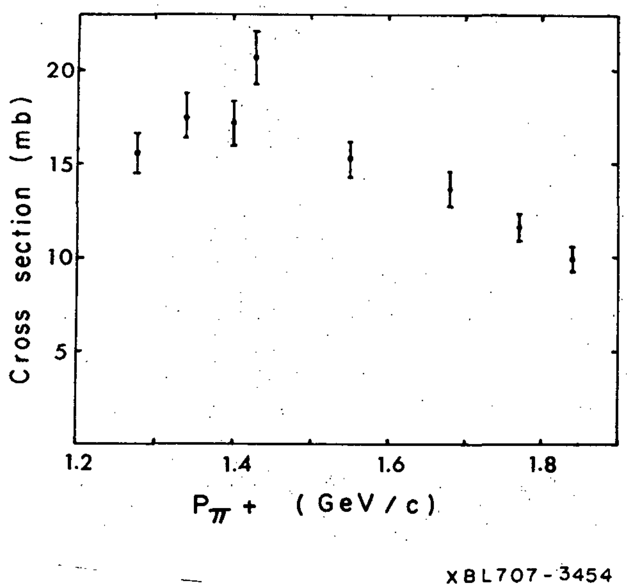

Fig. 4. Plot of total elastic cross section.

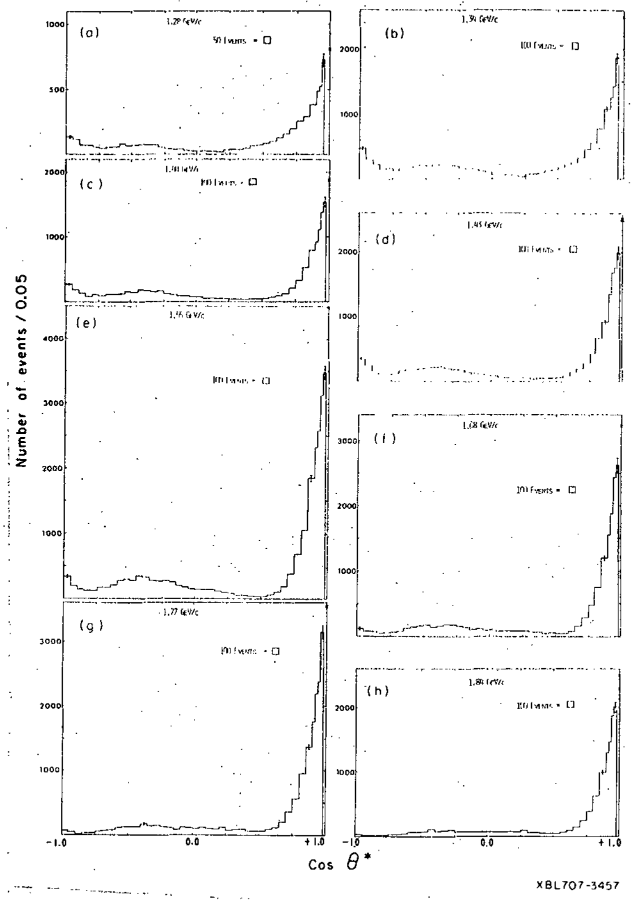

Fig. 5. Angular distributions. The $\times$ on the ordinate at $\cos\theta^* = 1$ is the point obtained from the extrapolation using the Legendre series. The events in the histogram are weighted. Typical errors are shown on some of the boxes. For the numbers and cross sections, see Table II.

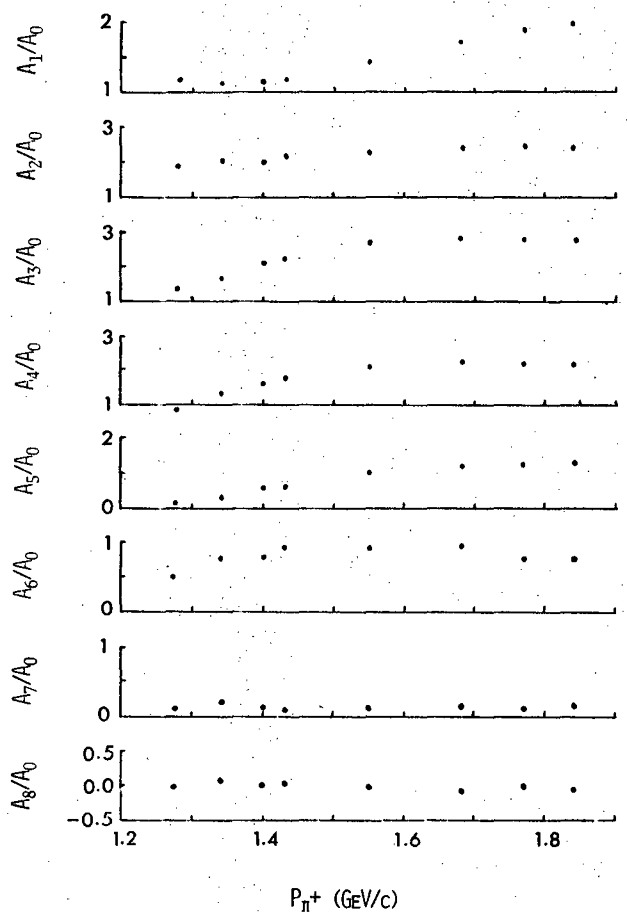

Fig. 6. Legendre coefficients normalized to A_0 for the eight-order fit. The errors are smaller than the size of the points (see Table IV). The difference in the coefficients between the eighth order and the minimum order necessary to fit the data was always less than the error in the coefficients.

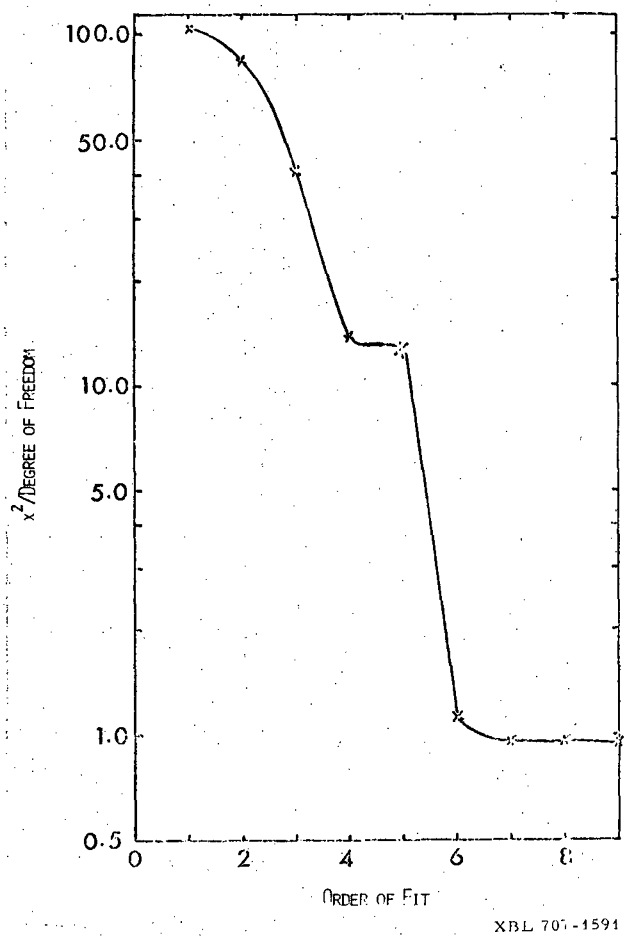

Fig. 7. Curve of χ^2 divided by degrees of freedom as a function of the order of fit for 1.43 GeV/c.

TECHNICAL INFORMATION DIVISION
LAWRENCE RADIATION LABORATORY
UNIVERSITY OF CALIFORNIA
BERKELEY, CALIFORNIA 94720